irradiance as a final step, the changes in atmospheric conditions between clear-sky days are not a major source of error in our final forecasts.

Next, we use the clear-sky indices to interpolate the scattered data onto a 1400 km^2 clear-sky index map for the Tucson region. To generate a clear-sky index map, we first create a 0.001° grid (with grid points approximately every 100 m) and add the sparse data from our network to the grid. We then set points along each boundary of the grid to the average of the clear-sky index values obtained from all the sensors. As we will see in Sections 4.4 and 5, this boundary condition helps to maintain forecast skill at longer time horizons.

Next, we fill all points in the grid with interpolated values as shown in Fig. 2. We chose to use multiquadric interpolation because it performs well at interpolating scattered geospatial data (Franke, 1982; Nuss and Titley, 1994), and it was more robust with our sparse data. We did not use a kriging method, even though kriging is often used to interpolate geospatial data, because we lack sufficient data to adequately estimate the variogram (Webster and Oliver, 1993; Sirayanone, 1988). We also explored inverse distance weighted interpolation, but found the output to be similar to multiquadric interpolation with insignificant differences in forecast errors (typically <3 W/m^2 difference in the root mean square error for all forecast horizons).

Then, we translate this interpolated clear-sky map a distance determined by the cloud motion vectors (which may vary in time). The translation in the x direction, with the y translation being analogous, is given by

$$\Delta x(t_i, t) = \int_{t_i}^{t} v_x(t')dt', \tag{2}$$

where t_i is the time at which the forecast is being made, $t - t_i$ is the forecast horizon, and $v_x(t)$ is the x component of the time-varying cloud motion vector. Any grid points that are missing data after the translation are filled with the average clear-sky index for all the sensors. Fig. 2 shows an example of an interpolated clear-sky index map and a map that has been shifted along the estimated cloud motion vector. Finally, we sample from this translated map at the desired forecast locations to obtain a forecasted clear-sky index which can be multiplied by the clear-sky expectation for that location to obtain an irradiance forecast. As we will discuss, for sufficiently long forecast horizons this procedure makes our network based forecasts indistinguishable from spatially-average persistence forecasts.

Forecasts out to 2 h in advance with 1 min time resolutions were made every 1 min for this analysis. As an example, one hour's worth of 5 min ahead forecasts along with measurements are shown in Fig. 3. This time-series is a composite showing snapshots (individual points) from 120 different forecasts that were each made 5 min in advance on a rolling basis. Concatenating points from different forecasts this way for several months lets us evaluate errors for forecasts with a 5 min horizon. Furthermore, updating forecasts every 1 min is valuable since 1 s data is constantly streaming into our database and each forecast has some new information that will likely improve the prediction for a specific time in the future. Later, we discuss errors as function of forecast horizon.

For estimating cloud motion velocity vector components (v_x, v_y), several techniques have been discussed including sensor correlations (Fung et al., 2014; Bosch et al., 2013), predictions from NWP (Lave and Kleissl, 2013; Lonij et al., 2013), analysis of aircraft communications addressing and reporting system (ACARS) or rawinsonde data, scaling of measured ground velocity, analysis of sky camera images (Urquhart et al., 2013), and analysis of satellite images (Hammer et al., 1999). For our analysis, we used modeled soundings (atmospheric temperature and

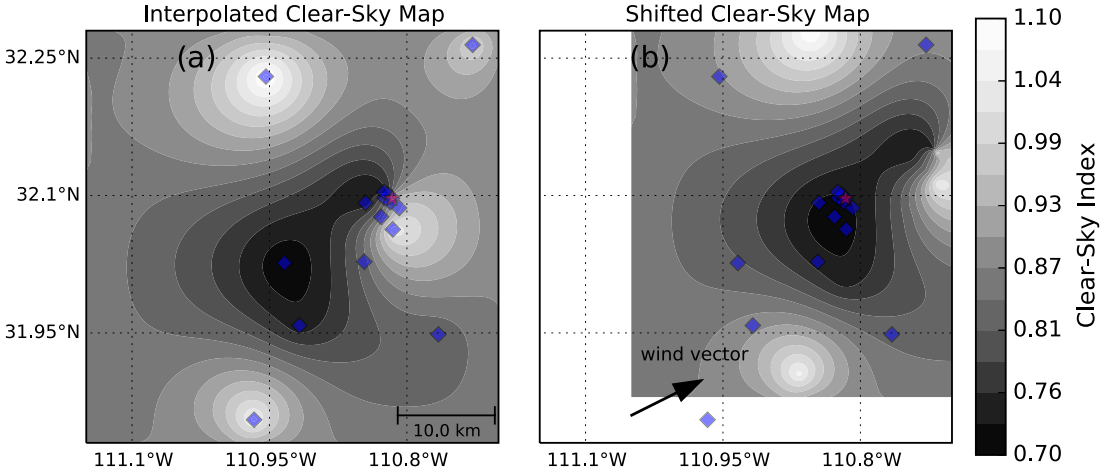

Fig. 2. An example interpolated map of clear-sky index on 5/19/14 near noon is shown in (a). Using the estimated cloud motion vectors this map is shifted according to desired forecast horizon as shown in (b). Then, samples from this shifted map are taken to as the forecasted clear-sky index for a particular location. The white space at bottom and left of (b) is filled in with the average clear-sky index of all sensors at the time the forecast is generated. The red star indicates the sensor that was used to evaluate forecasts. (For interpretation of the references to color in this figure legend, the reader is referred to the web version of this article.)